Site symmetry and crystal field of Ce^{3+} luminescent centres in $KMgF_3$

2001 J. Phys.: Condens. Matter 13 3461

(http://iopscience.iop.org/0953-8984/13/14/318)

INSTITUTE OF PHYSICS PUBLISHING JOURNAL OF PHYSICS: CONDENSED MATTER

J. Phys.: Condens. Matter **13** (2001) 3461–3473 www.iop.org/Journals/cm PII: S0953-8984(01)21603-8

Site symmetry and crystal field of Ce^{3+} luminescent centres in $KMgF_3$

M Yamaga[1], M Honda[2], N Kawamata[2], T Fujita[3], K Shimamura[3] and T Fukuda[3]

[1] Department of Electrical and Electronic Engineering, Faculty of Engineering, Gifu University, Gifu 501-1193, Japan
[2] Faculty of Science, Naruto University of Education, Naruto 772-8502, Japan
[3] Institute for Materials Research, Tohoku University, Sendai 980-8577, Japan

Received 12 March 2001

Abstract

The electron-spin resonance (ESR) spectra of Ce^{3+} in $KMgF_3$ observed at low temperatures (<20 K) show that two tetragonal and two orthorhombic Ce^{3+} centres exist in the absence of a cubic centre. These Ce^{3+} centres are strongly associated with substitution of Ce^{3+} ions for K^+ ions with K^+-ion vacancies at three different sites and for a Mg^{2+} ion with a vacancy of the nearest neighbour Mg^{2+} ion along the [101] direction as charge compensators.

The optical absorption spectrum of Ce^{3+} in $KMgF_3$ measured at room temperature consists of two intense broadbands with peaks at 229 and 237 nm, and two weak bands with peaks at 203 and 211 nm corresponding to the transition from the ground state $^2F_{5/2}$ to the $5d^1$ excited states of Ce^{3+}. The Ce^{3+} luminescence spectrum excited at 229 or 237 nm at room temperature is composed of broadbands with double peaks at 265 and 282 nm, which are due to the ground-state splitting between $^2F_{5/2}$ and $^2F_{7/2}$. The peak of the weak luminescence band excited at a tail (250–280 nm) of the intense absorption bands is shifted to lower energy. The intense and weak Ce^{3+} luminescence bands are assigned to Ce^{3+} ions substituting for K^+ ions away from and near to K^+-ion vacancies, respectively. The luminescence from Ce^{3+} ions substituting for Mg^{2+} ions could not be observed at room temperature.

1. Introduction

Recently, operations of optically pumped tunable solid-state lasers in the UV region using the $5d$–$4f$ transition of Ce^{3+} in fluoride crystals $LiYF_4$ [1,2] and $LiCaAlF_6$ [3] were reported. As energy levels of the $5d^1$ excited states of Ce^{3+} in crystals are strongly affected by symmetry and strength of the Ce^{3+} crystal field, the optical transitions are assigned to shift from the UV into visible regions by varying host crystals [4]. New Ce^{3+}-activated fluoride crystals capable of lasing with wider UV tunability, $SrAlF_5$ [5], $BaLiF_3$ (BLF) [6–9], $KMgF_3$ (KMF) [10,11], BaF_2 [12] and $BaMgF_4$ [13] were grown and their spectroscopic features were reported.

In a previous paper [7], we reported three distinct luminescent centres of Ce^{3+} in the BLF crystal. UV excitation at 248 nm produces an intense luminescence band (A) with a peak at ∼320 nm and a large Stokes shift (∼8300 cm^{-1}) and a weak band (C) with a peak at ∼280 nm and a Stokes shift energy of half that amount (∼4400 cm^{-1}) [6,7,9]. In addition, UV excitation at 280 nm produces the other weak luminescence band (B) with a peak at ∼340 nm and a large Stokes shift (∼7800 cm^{-1}). The Ce^{3+} ions substitute for Ba^{2+} ions in BLF, being accompanied by charge compensators [7,8]. The A and C luminescent centres are assigned to Ce^{3+} with the Li substitution at the nearest neighbour Ba^{2+} sites along the [001] and [110] directions, respectively. The B centre is assigned to Ce^{3+} with a Ba^{2+} vacancy near to Ce^{3+}.

The KMF crystal has the same structure with symmetry O_h as the BLF crystal. The weak and intense Ce^{3+} luminescence bands excited at 234 and 271 nm in KMF, respectively, were observed at 275 and 350 nm. The two Ce^{3+} luminescent centres were assigned to Ce^{3+} ions unperturbed and perturbed by two K^+-ion vacancies [10].

This paper describes the growth of Ce^{3+}-doped single KMF crystals, characterization of the electronic states and identification of Ce^{3+} in this crystal using optical and electron-spin resonance (ESR) techniques. We discuss the difference between the Ce^{3+} luminescent centres in KMF and BLF with the same crystal structure on terms of symmetry and strength of the Ce^{3+} crystal field.

2. Experimental procedure

The KMF crystal has the cubic perovskite structure with space group O_h^1 and the lattice constant of $a = 3.989$ Å. Ce^{3+}-doped KMF crystals were grown in a vacuum-tight Czochralski system equipped with a graphite heater and automatic control of boule diameter. As KMF melts incongruently, a single crystal must be grown from a non-stoichiometric melt to avoid other phase precipitation. The starting charges were formed from a non-stoichiometric mixture of KF(54 mol%) and MgF_2(46 mol%). The compounds were melted and soaked in a furnace under a reactive atmosphere of CF_4. The crystals were grown along the crystalline c-axis at a pulling rate of 1 mm h^{-1} and a rotation rate of 15 rpm. The composition determined by the inductively coupled plasma (ICP) technique is represented by $K_{0.995}Mg_{0.987}F_{2.969}$. As the ICP signals of Ce^{3+} were observed within the limit of the measurement sensitivity, the segregation coefficient of Ce^{3+} in the crystals was expected to be a low value of <0.01.

Laue x-ray diffraction was used to produce oriented samples, which were cut parallel to the crystalline a-, b- and c-axes. The samples were prepared for optical and ESR measurements by polishing their faces using diamond paste impregnated laps.

ESR measurements of Ce^{3+} in KMF were made in the temperature range of 5–20 K using a Bruker EMX10/12 X-band spectrometer with microwave frequencies of 9.686–9.698 GHz, a microwave power of 1 mW and 100 kHz field modulation. The angular variations of the ESR spectra were measured by rotating a sample in a cavity.

The optical absorption spectra of Ce^{3+} in KMF were measured in the range of 180–2500 nm at room temperature using a Hitachi U-3500 spectrophotometer. The luminescence and excitation spectra of Ce^{3+} were measured in the range of 200–900 nm at room temperature using a Hitachi F-4500 fluorescence spectrophotometer. The lifetime of the Ce^{3+} luminescence was measured using a Horiba NAES-700F time-resolved photoluminescence spectrometer at room temperature at the Instrumental Analysis Center, Gifu University.

3. Experimental results

3.1. ESR spectra

Figure 1 shows the ESR spectra of Ce^{3+} in the KMF crystal measured in the temperature range of 5–18 K with a microwave frequency of 9.688 GHz and magnetic field $\boldsymbol{B}$ parallel to the crystalline [010]-axis. The spectrum observed at 5 K consists of several resonance lines denoted by T_1, R_1 and R_2. As temperature increases gradually, their signal intensities are drastically decreased, and disappear above 15 K. The line at $B \sim 1.3$ T below 6 K, denoted by T_2, is very weak and asymmetric in shape. Above 8 K, the line shape is changed to symmetric. The intensity has a maximum at ~10 K and disappear above ~20 K. The different temperatures where the ESR signals disappear suggest the existence of various Ce^{3+} centres in the KMF crystal. The sharp and complex ESR signals observed at 0.14–0.17 T and 0.29–0.31 T are due to cavity impurities.

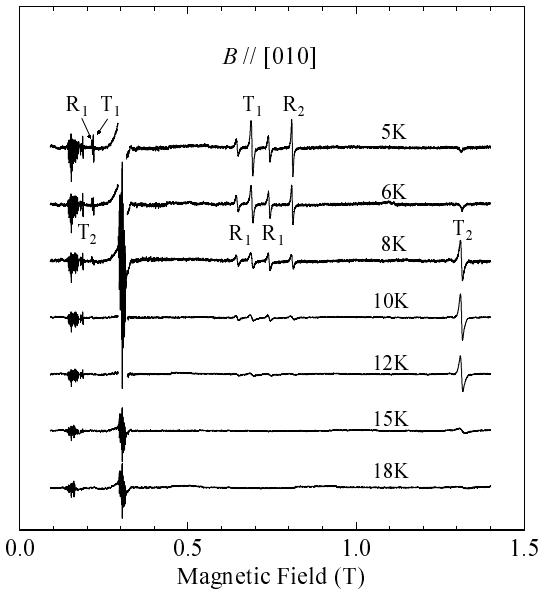

Figure 1. The temperature dependence of the ESR spectra of Ce^{3+} in $KMgF_3$ with $\boldsymbol{B} \parallel [010]$, a microwave frequency of 9.688 GHz and a microwave power of 1 mW. Four distinct ESR signals are denoted by T_1, T_2, R_1 and R_2.

The angular variations of the ESR spectra were observed at 5 K and 10 K for magnetic field rotations in the (100)- and (110)-planes. The angular variations were very complicated. However, the variations could be followed by taking account of the different relative intensities between the four Ce^{3+} centres at 5 and 10 K. Figure 2 shows the angular variations of the g-values calculated for the four Ce^{3+} centres using $h\nu = g\mu_B BS$ where h is the Plank constant, μ is microwave frequencies of 9.686–9.698 GHz, μ_B is the Bohr magneton, B is a resonance magnetic field and $S(= \frac{1}{2})$ is an effective spin for Ce^{3+} ions. The angular variation patterns of the (T_1, T_2) and (R_1, R_2) lines show tetragonal and orthorhombic symmetry, respectively. The orientation dependences of the g-values in figure 2 are analysed using an effective Hamiltonian appropriate to orthorhombic symmetry [14],

$$\mathcal{H} = \mu_B g_x B_x S_x + \mu_B g_y B_y S_y + \mu_B g_z B_z S_z. \tag{1}$$

In the case of tetragonal symmetry, the relation of $g_\parallel = g_z$ and $g_\perp = g_x = g_y$ is satisfied. The principal x-, y- and z-axes for the tetragonal centres (T_1, T_2) and orthorhombic centre R_2, respectively, are the ([100], [010], [001]) and ([10$\bar{1}$], [010], [101]) axes of the crystal. The principal z- and x-axes for the R_1 centre are rotated in the (010) plane with an amount of $\pm 9^\circ$ from the [001] and [100] directions, respectively, and the y-axis is the [010] direction. The full curves in figure 2 calculated using equation (1) with the g-values for T_1, T_2, R_1 and R_2 given in table 1, are in good agreement with the experimental points. In table 1, the g-values of Ce^{3+} in KMF [11] and BLF [8] are added in comparison.

Table 1. The spin-Hamiltonian parameters in equation (1) for Ce^{3+} in $KMgF_3$ in comparison with those in $BaLiF_3$.

Crystals	T_1	T_2	R_1	R_2	Reference
$KMgF_3$	$g_\parallel = 3.167(2)$	$g_\parallel = 3.699(2)$	$g_z = 3.253(4)$	$g_z = 2.635(4)$	This work
			$z \parallel [001] \pm 9^\circ$ [a]	$z \parallel [101]$	
	$g_\perp = 1.002(3)$	$g_\perp = 0.527(1)$	$g_x = 0.962(4)$	$g_x = 0.481(6)$	
			$x \parallel [100] \pm 9^\circ$ [a]	$x \parallel [\bar{1}01]$	
			$g_y = 0.933(2)$	$g_y = 0.854(1)$	
			$y \parallel [010]$	$y \parallel [010]$	
	$\tilde{g} = 1.724$ [b]	$\tilde{g} = 1.584$ [b]	$\tilde{g} = 1.716$ [b]	$\tilde{g} = 1.323$ [b]	
$KMgF_3$	$g_\parallel = 3.178(5)$		$g_z = 3.785(5)$	$g_z = 2.634(5)$	[11]
			$z \parallel [101]$	$z \parallel [101]$	
	$g_\perp = 1.004(5)$		$g_x = 0.38(1)$	$g_x = 0.51(1)$	
			$x \parallel [\bar{1}01]$	$x \parallel [\bar{1}01]$	
			$g_y = 0.739(5)$	$g_y = 0.854(5)$	
			$y \parallel [010]$	$y \parallel [010]$	
	$\tilde{g} = 1.729$ [b]		$\tilde{g} = 1.635$ [b]	$\tilde{g} = 1.333$ [b]	
$BaLiF_3$	$g_\parallel = 2.866(6)$	$g_\parallel = 0.772(4)$	$g_z = 0.889(7)$	$g_z = 1.152(6)$	[8]
			$z \parallel [001]$	$z \parallel [001]$	
	$g_\perp = 1.196(1)$	$g_\perp = 2.465(1)$	$g_x = 2.214(2)$	$g_x = 2.079(5)$	
			$x \parallel [110]$	$x \parallel [110]$	
			$g_y = 2.141(2)$	$g_y = 1.580(4)$	
			$y \parallel [\bar{1}10]$	$y \parallel \bar{1}10]$	
	$\tilde{g} = 1.753$ [b]	$\tilde{g} = 1.901$ [b]	$\tilde{g} = 1.748$ [b]	$\tilde{g} = 1.604$ [b]	

[a] The principal z- and x-axes are rotated with an amount of $\pm 9^\circ$ from [001] and [100].
[b] $\tilde{g} = \frac{1}{3}(g_\parallel + 2g_\perp)$, $\frac{1}{3}(g_x + g_y + g_z)$.

3.2. Optical spectra

Figure 3 shows the absorption spectrum of Ce^{3+} in KMF in comparison with that in BLF. This spectrum consists mainly of two spectral groups; one is two intense bands with peaks at 229 and 237 nm: the other is two weak bands with peaks at 203 and 211 nm. An additional weak band appears at a tail of the intense bands in lower energy. Although the line shape in KMF is the same as that in BLF [7], the peaks are slightly shifted to higher energy than in BLF.

UV excitation in the range of 200–235 nm produces intense luminescence bands with double peaks in figure 4(a). Weak luminescence bands appear around ~300 nm when the excitation wavelength is above 250 nm. The Ce^{3+} luminescence spectrum from a single Ce^{3+} site should be decomposed into two Gaussians with the energy separation of 2200 cm^{-1}, being equal to the ground-state splitting between $^2F_{5/2}$ and $^2F_{7/2}$ of Ce^{3+}. The luminescence spectrum at λ_{ex} =235 nm is decomposed into two Gaussians with the peaks at 265 and 282 nm

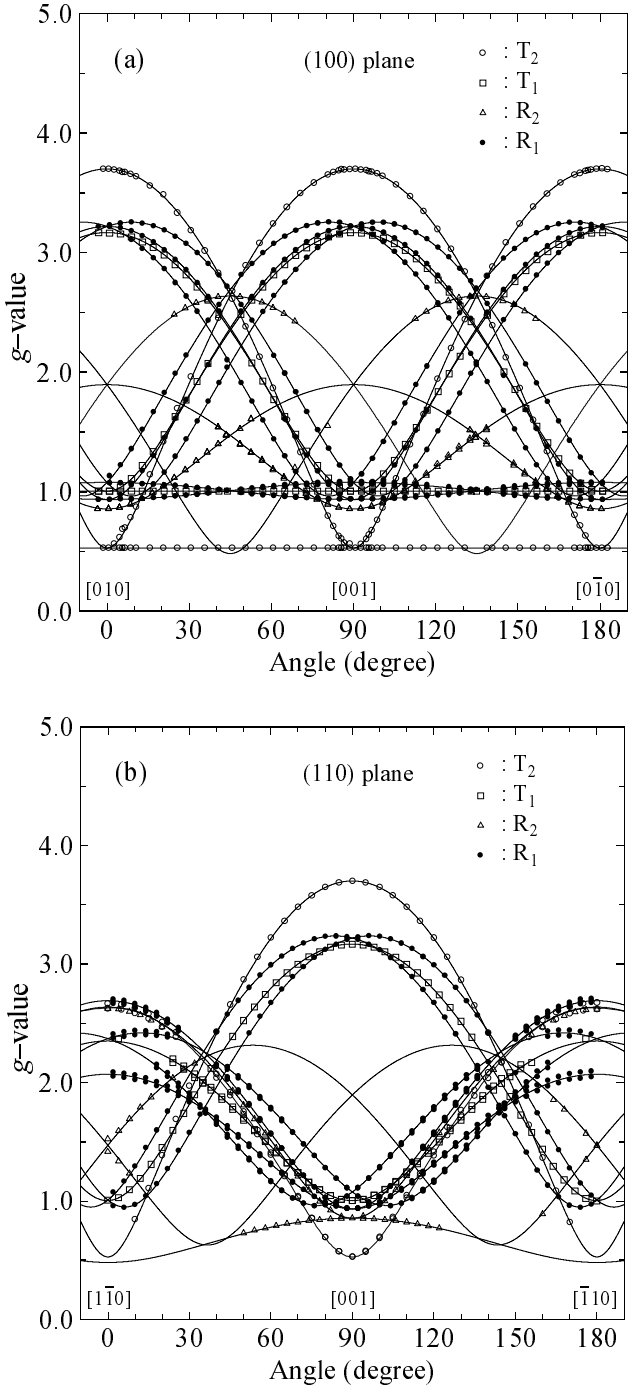

Figure 2. The angular variations of the g-values of the ESR lines, T_1, T_2, R_1 and R_2, observed with microwave frequencies of 9.686–9.698 GHz in (a) the (100) plane and (b) the (110) plane. Solid curves are calculated using equation (1) and the spin-Hamiltonian parameters in table 1.

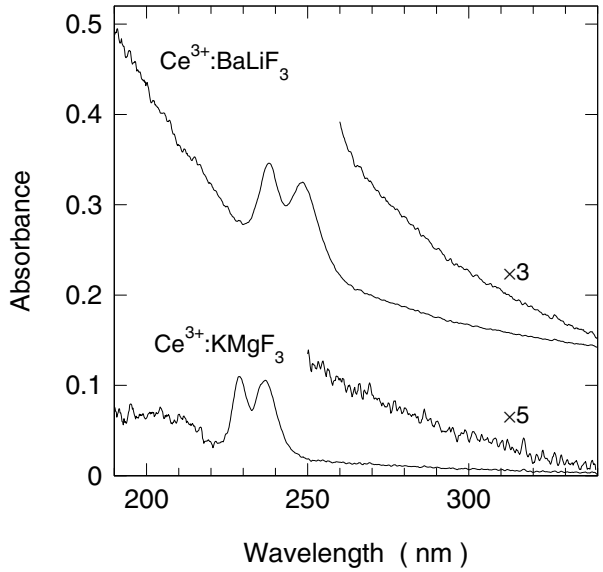

Figure 3. The absorption spectrum of Ce^{3+} in $KMgF_3$ measured at room temperature in comparison with that in BLF with a shifted background level [7].

denoted by C_1 and C_2, the energy separation being $\sim$2200 cm^{-1}. The luminescence spectrum at λ_{ex} =260 nm is decomposed into three Gaussians. Two dominant components at 297 and 316 nm and a very weak component at 347 nm are denoted by B_1, B_2 and D. The energy separation of the B_1 and B_2 bands is $\sim$2100 cm^{-1}. The additional D band at 347 nm is coincident with that in KMF observed by Francini *et al* [10].

The excitation spectra were measured in the luminescence wavelength range of 250–340 nm as shown in figure 4(b). The excitation spectrum of the C_1 band at λ_{em} =270 nm is coincident with the absorption spectrum in figure 3. The excitation spectrum for a tail (λ_{em} = 330 nm) of the B_1/B_2 bands consists of four bands at 203, 227, 236 and 247 nm. Although the three peak wavelengths are nearly equal to those in the C_1 excitation spectrum, the relative intensities are reverse. The position of 330 nm is far away from the C_1/C_2 bands as shown in figure 4(a). These results indicate that the excitation spectrum at λ_{em} = 330 nm may be associated with the B_1/B_2 luminescence bands. As a Stokes shift energy is defined as energy separation between the lowest-energy excitation (absorption) band and the luminescence band, it is obtained to be 4500 and 6800 cm^{-1} for the C_1 and B_1 luminescence bands, respectively.

These line shapes of the luminescence and excitation spectra of Ce^{3+} in KMF are very similar to those in BLF [7] except for the peak wavelengths. In consequence, the C_1/C_2 and B_1/ B_2 luminescence bands are assigned to two distinct Ce^{3+} centres with the same ligand coordination as in BLF.

Figure 5 shows the decay curve of the C_1 luminescence at 270 nm with an excitation wavelength of 235 nm at room temperature. The lifetime is obtained to be 20 ns. The decay curve of the B_1/B_2 luminescence could not be observed at room temperature because the fairly weak intensity was obscured by scattering of the excitation beam.

Figure 6 shows the lifetimes of the C_1/C_2 luminescence bands and the intensities integrated in a time domain as a function of the wavelength measured at room temperature. The lifetime is nearly constant in the whole spectral range within the experimental errors. The intensity

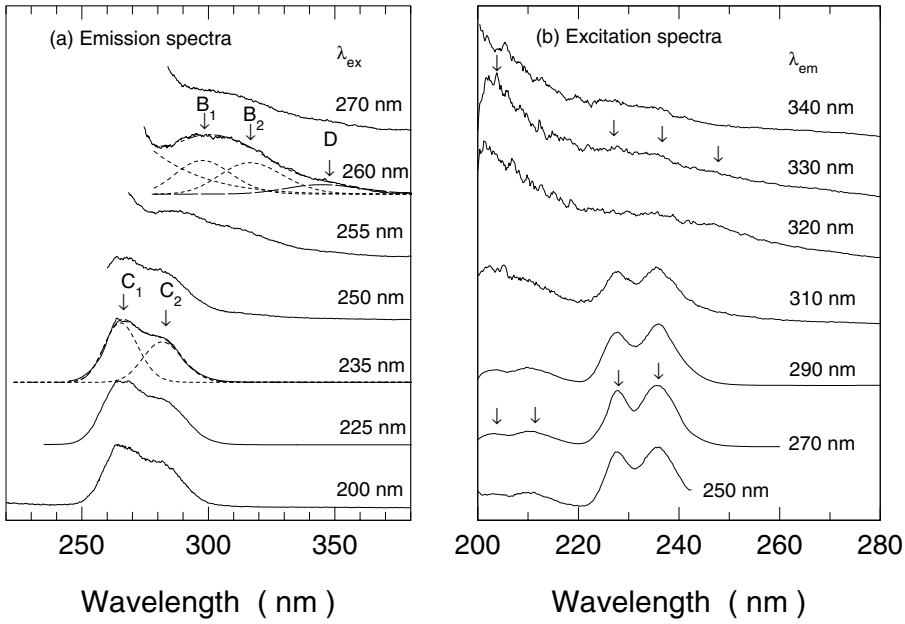

Figure 4. (a) The luminescence spectra of Ce^{3+} in $KMgF_3$ excited with different wavelengths. (C_1, C_2), (B_1, B_2) and D denote different Ce^{3+} luminescent centres. The dotted curves for the spectra at $\lambda_{ex} = 235$ and 260 nm represent deconvoluted Gaussians. (b) The excitation spectra obtained by monitoring the intensities of the Ce^{3+} luminescence at different fixed wavelengths. Arrows show the peak positions of the excitation bands for the C_1/C_2 and B_1/B_2 luminescence bands.

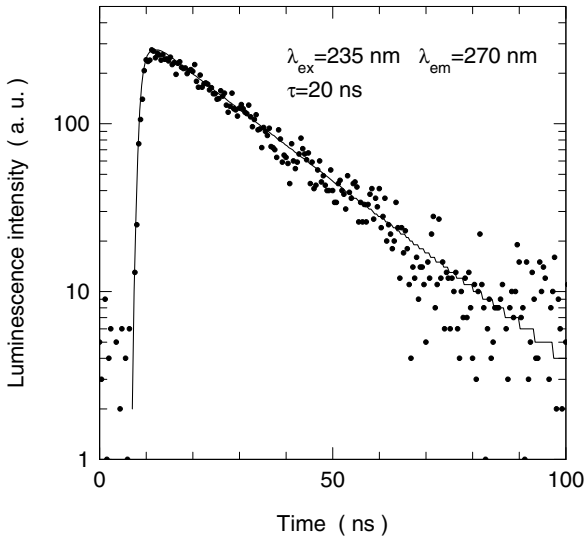

Figure 5. The decay curve of the C_1 luminescence band ($\lambda_{ex} = 235$ nm, $\lambda_{em} = 270$ nm). The solid curve is calculated by convolution of a single exponential and pulse shape of the excitation beam. The lifetime is obtained to be 20 ns.

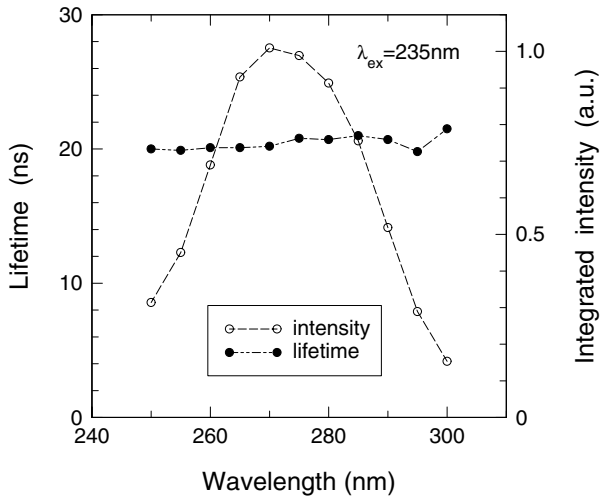

Figure 6. The lifetimes of the C_1/C_2 luminescence and the intensities integrated in a time domain as a function of the wavelength at room temperature.

spectrum is similar to the line shape of the C_1/C_2 luminescence as shown in figure 4(a). These results are in agreement with those obtained in Ce^{3+}-doped $LiCaAlF_6$ where Ce^{3+} ions occupy the ordinary Ca^{2+} sites [15].

4. Discussion

4.1. Symmetry of Ce^{3+} centres

The KMF crystal structure is shown in figure 7. A K^+ cubo-octahedron consists of twelve F^- ligands classified as two groups, one containing eight ligands in a cube and the other containing four ligands in an octahedron that lacks two ligands on the crystalline [001]-axis. A Mg^{2+} ion forms an octahedron composed of six F^- ligand ions. The ionic radius of K^+ in a twelve-fold coordination is 1.74 Å, whereas that of Mg^{2+} in a six-fold coordination is 0.86 Å [16]. The ionic radii of Ce^{3+} in twelve-fold and six-fold coordinations are 1.43 Å and 1.15 Å, respectively [16]. Substitution of Ce^{3+} for Mg^{2+} may be less probable because of ionic size mismatch. Then, Ce^{3+} ions are expected to substitute for K^+ ions. However, the substitution of Ce^{3+} in KMF should be determined experimentally—for example, by the ESR technique.

First, we discuss the difference in the electronic properties of Ce^{3+} in twelve-fold and six-fold coordinations.

(i) In a cubic crystal field, the ground state $^2F_{5/2}$ of Ce^{3+} splits into a doublet Γ_7 and a quartet Γ_8. The ground state in a twelve-fold coordination is Γ_8, whereas that in a six-fold coordination is Γ_7. The mean g-values for Γ_8 and Γ_7 are 2 and 10/7, respectively [11,17]. Then, they can determine whether Ce^{3+} complexes are twelve-fold or six-fold coordinated.

(ii) The excited state ^2D_J of Ce^{3+} in a cubic field splits into (Γ_7, Γ_8) and Γ_8. Assuming that H_{s-o} (spin-orbit interaction) $<< H_{cub}$ (cubic crystal field), the $5d^1$ excited orbitals split into a doublet e_g and a triplet t_{2g}. The splitting of the $5d^1$ excited state in twelve-fold and six-fold coordinations are also in an opposite sense; that is, the lower excited states in twelve-fold and six-fold coordinations are e_g and t_{2g}, respectively [18].

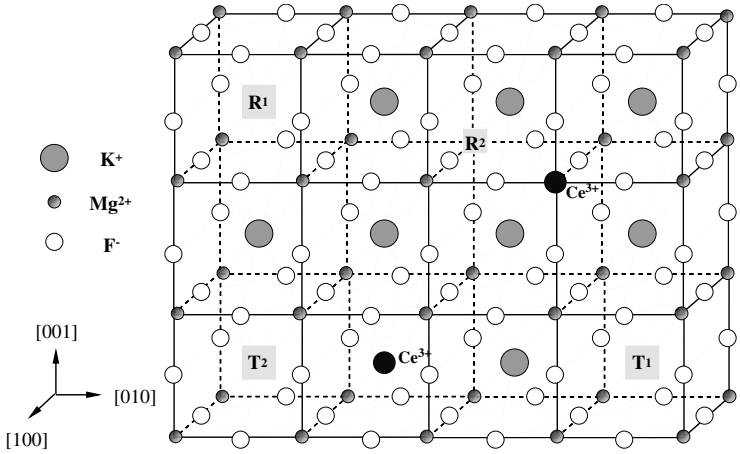

Figure 7. Models of the Ce^{3+} luminescent centres in $KMgF_3$

As the valence of Ce^{3+} ions has an excess charge of +2 and +1 for K^+ and Mg^{2+} ions, respectively, substitution of Ce^{3+} in the KMF crystal requires charge compensators. For the substitution of Ce^{3+} for K^+, the possible mechanisms of the charge compensation are as follows as; (i) a vacancy is created at the nearest Mg^{2+} site: (ii) two K^+ vacancies compensate for a single Ce^{3+} ion: (iii) F^- ions occupy interstitially, and (iv) O^{2-} impurity ions occupy F^- sites. The mechanism (iv) is less probable because of the crystal growth under a CF_4 atmosphere, that is, an oxygen-free atmosphere. The substitution of Ce^{3+} for Mg^{2+} also requires K^+ and/or Mg^{2+} vacancies as charge compensators. These charge compensators reduce Ce^{3+} complexes from cubic to lower symmetry. We discuss the g-values of the Ce^{3+} centres observed in KMF, taking account of symmetry and ligand coordination of the Ce^{3+} complexes.

4.1.1. Tetragonal The observed g-values for T_1 in table 1 is $(g_\parallel, g_\perp) = (3.167, 1.002)$. The approximate values of $g_\parallel = g_z$ and $g_\perp = \frac{1}{2}(g_x + g_y)$ for R_1 are set to $(g_\parallel, g_\perp) = (3.253, 0.948)$. Their g-values are very similar to each other. Further, the mean g-values for T_1 and R_1 are 1.724 and 1.716, respectively, being slightly less than 2, so that these Ce^{3+} ions are expected to be twelve-fold coordinated.

The ground state Γ_8 splits into Γ_6 and Γ_7 in a weak tetragonal field ($H_{tet} << H_{cub}$). The eigenfunctions of Γ_6 and Γ_7 are represented by [11,14]

$$\Gamma_6 \rightarrow |\tfrac{5}{2},\ \pm\tfrac{1}{2}\rangle$$

$$\Gamma_7 \rightarrow \mp\tfrac{1}{\sqrt{6}}\left(\sqrt{5}|\tfrac{5}{2},\ \mp\tfrac{5}{2}\rangle + |\tfrac{5}{2},\ \pm\tfrac{3}{2}\rangle\right).$$

The g-values for Γ_6 and Γ_7 are calculated to be $(g_\parallel,\ g_\perp) = (6/7, 18/7)$ and (22/7, 10/7), respectively [11,14]. The observed g-values for T_1 and R_1 are very close to the g-values calculated for Γ_7.

The observed g-values $(g_\parallel,\ g_\perp) = (3.699,\ 0.527)$ for T_2 are close to the average of the g-values, $(g_\parallel, g_\perp) = (30/7,\ 0)$ and $(18/7, 0)$, calculated for $|\frac{5}{2},\ \pm\frac{5}{2}\rangle$ and $|\frac{5}{2},\ \pm\frac{3}{2}\rangle$, respectively. The mean g-value is 1.584. These results mean that a strong tetragonal crystal field interaction mixes two Γ_7 states of $^2F_{5/2}$, resulting in that the mean g-value in the twelve-fold coordination is shifted from 2 to 10/7.

The mixing eigenfunction of the ground state is represented by a linear combination of $|\frac{5}{2},\ \mp\frac{5}{2}\rangle$ and $|\frac{5}{2},\ \pm\frac{3}{2}\rangle$, i.e. [8,11,14],

$$|\pm\tilde{\tfrac{3}{2}}\rangle = \cos\theta|\tfrac{5}{2},\ \mp\tfrac{5}{2}\rangle + \sin\theta|\tfrac{5}{2},\ \pm\tfrac{3}{2}\rangle. \tag{2}$$

The g-values for $|\pm\tilde{\frac{3}{2}}\rangle$ are calculated to be [8,11,14]

$$g_\parallel = \tfrac{6}{7}|5\cos^2\theta - 3\sin^2\theta| \tag{3}$$

$$g_\perp = \tfrac{6}{7}|2\sqrt{5}\cos\theta\sin\theta|. \tag{4}$$

The g-values $(g_\parallel, g_\perp) = (3.99,\ 0.78)$ calculated using equations (3) and (4) with $\theta = 12^\circ$ are slightly larger than the observed values. The difference in the observed and calculated g-values can be explained by further mixing $|\frac{7}{2}, \mp\frac{5}{2}\rangle$ and $|\frac{7}{2}, \pm\frac{3}{2}\rangle$ of the first excited state $^2F_{7/2}$ through the second-order perturbation [8]. The modified eigenfunction in equation (2) is represented by

$$|\pm\tilde{\tfrac{3}{2}}'\rangle = p_1|\tfrac{5}{2},\ \mp\tfrac{5}{2}\rangle + q_1|\tfrac{5}{2},\ \pm\tfrac{3}{2}\rangle \pm r_1|\tfrac{7}{2},\ \mp\tfrac{5}{2}\rangle \pm t_1|\tfrac{7}{2},\ \pm\tfrac{3}{2}\rangle \tag{5}$$

where $p_1^2 + q_1^2 + r_1^2 + t_1^2 = 1$. The g-values $(g_\parallel, g_\perp) = (3.70, 0.53)$ calculated for $|\pm\tilde{\frac{3}{2}}'\rangle$ with $(p_1, q_1, r_1, t_1) = (0.97, 0.13, -0.02, -0.23)$ in equation (5) and the g-values formulas in [8] fit the observed g-values quite well.

4.1.2. Orthorhombic The observed g-values for R_2 in table 1 are $(g_z,\ g_x,\ g_y) = (2.635,\ 0.481,\ 0.854)$. The mean g-value of 1.323 is slightly smaller than that (1.43) calculated for the ground state Γ_7 in a six-fold coordination [11,14],

$$\Gamma_7 \rightarrow \tfrac{1}{\sqrt{6}}\left(|\tfrac{5}{2},\ \pm\tfrac{5}{2}\rangle - \sqrt{5}|\tfrac{5}{2}, \mp\tfrac{3}{2}\rangle\right).$$

This result suggests a possibility that Ce^{3+} ions substitute for Mg^{2+} ions. The eigenfunction of the Hamiltonian of the crystal field including an orthorhombic distortion is assumed to be [8,11,14,19],

$$|\pm\tilde{\tfrac{1}{2}}'\rangle = p_2|\tfrac{5}{2},\ \pm\tfrac{5}{2}\rangle + q_2|\tfrac{5}{2},\ \mp\tfrac{3}{2}\rangle + r_2|\tfrac{5}{2},\ \pm\tfrac{1}{2}\rangle \tag{6}$$

where $p_2^2 + q_2^2 + r_2^2 = 1$. The g-values of $(g_z, g_x, g_y) = (2.65, 0.47, 0.93)$ calculated using equation (6) with $(p_2,\ q_2,\ r_2) = (0.76, -0.24, 0.60)$ and the g-values formulas in [8] are in agreement with the observed values.

4.2. Identification of Ce^{3+} centres

The summary of the ESR results and proposed models of the Ce^{3+} centres are as follows:

(i) The mean g-values for T_1, R_1, and T_2 suggest that Ce^{3+} ions are twelve-fold coordinated; that is, the Ce^{3+} ions substitute for K^+ ions. The g-values for T_1 and R_1 show that the Ce^{3+} complexes have weak tetragonal and orthorhombic distortions, being approximately cubic. The $g_\perp$ ESR line shape for T_2 has only negative component of the derivative line below 6 K and becomes symmetric above 8 K as shown in figure 1. An asymmetric line shape of the resonance is usually measured under conditions of adiabatic rapid passage, in which a sweep rate of magnetic field is much faster than a spin-lattice relaxation rate [20]. As the spin-lattice relaxation rate is enhanced with an increase of temperature, the line shape changes from asymmetric to symmetric at higher temperatures. This indicates that the spin-lattice relaxation rate for T_2 is smaller than those for T_1 and R_1. Therefore, T_2 is

due to Ce^{3+} complexes more strongly distorted along the [001] direction than T_1. Models of T_1, R_1 and T_2 are shown in figure 7. The tetragonal distortions for T_1 and T_2 are created by K^+ vacancies along the [001] direction, where the distances between Ce^{3+} and the vacancies are $2a$ and a (a: lattice constant), respectively. A K^+-ion vacancy along the [102] direction may tilt the principal z-axis slightly from the [001] direction. Assuming that the magnitudes of the distortions for T_1 and R_1 are similar to each other, R_1 corresponds to Ce^{3+} with a K^+-ion vacancy with the $[0\bar{1}2]$ direction in figure 7.

(ii) Ibragimov *et al* [11] reported another orthorhombic Ce^{3+} centre with the principal z-axis parallel to the [101] direction and the g-values of $(g_z, g_x, g_y) = (3.785, 0.38, 0.739)$, being very close to those for T_2, as shown in table 1. Here, the orthorhombic centre is denoted by R_1' in order to distinguish this centre from our R_1 centre. The mean g-value of 1.635 suggests that R_1' is assigned to Ce^{3+} substituting for K^+. They have proposed a model that R_1' corresponds to a Ce^{3+} complex accompanied by an O^{2-} ion substituting for one of four F^- ligand ions in the (010) plane containing Ce^{3+} [11]. Such R_1' ESR signals could not be observed in our KMF crystals because our samples were grown in a CF_4 atmosphere, that is, an oxygen-free atmosphere.

(iii) As the mean g-value of R_2 is 1.324, R_2 is assigned to Ce^{3+} complexes in a six-fold coordination. The principal z-axis is parallel to the [101] direction. These results lead us to deduce that R_2 is assigned to substitution of Ce^{3+} for Mg^{2+} with a vacancy at the nearest neighbour Mg^{2+} sites along the [101] direction or with an interstitial F^- ion in the (010) plane including the Ce^{3+} ion [11]. The vacancy model may be more probable because the model is expected to make more space around the substitutional Mg^{2+} site than the interstitial model. Although substitution of Ce^{3+} for ordinary Mg^{2+} sites is less probable because of ionic size mismatch, such a Mg^{2+}-ion vacancy may enlarge the possibility.

(iv) There are other two possible charge-compensation mechanisms: (1) a vacancy at a Mg^{2+} site along the [111] direction and (2) two K^+ vacancies for a single Ce^{3+} as discussed in section 4.1. Case (1) produces a trigonal distortion. However, no ESR signals with trigonal symmetry could be observed within the limit of the measurement sensitivity. The same result was obtained in Ce^{3+}:BLF [8]. Case (2) has several configurations between two K^+-ion vacancies. For example, there are two configurations of K^+ vacancies created at two of six nearest neighbour K^+ sites along the [100], [010], and [001] directions; one corresponds to vacancies located along the [100] and [010] directions with a right angle: the other corresponds to vacancies along the [001] and $[00\bar{1}]$ directions with opposite sides. The relative probabilities of the vacancy production are 4:1. The Ce^{3+} complexes with these vacancies show the same orthorhombic and tetragonal symmetry as R_2 and T_2 in KMF. However, the g-values analyses in above sections 4.1 and 4.2 exclude the possibility that they correspond to R_2 and T_2. Another combinations of two K^+-ion vacancies near to Ce^{3+} give rise to complicated angular variations of the ESR spectra. Such ESR signals could not be observed in the experimental errors.

4.3. Optical spectra and crystal field

The observed absorption spectrum of Ce^{3+} in KMF indicates that the lower excited state is the ^2E_g state, being further split into two Kramers doublets by the second-order perturbation of the spin-orbit interaction and a low-symmetry distortion, for example, a tetragonal distortion. The Stokes shift energy ($\sim$4500 cm^{-1}) of the C_1 luminescence in KMF is close to that ($\sim$4400 cm^{-1}) for the C_1 luminescence in BLF [7] and slightly larger than that ($\sim$3100 cm^{-1}) in $LiYbF_4$ [21]. The lifetimes of the C_1/C_2 bands are nearly constant in the whole spectral range. These optical results deduce that Ce^{3+} ions with nearly cubic symmetry occupy ordinary K^+

sites away from K^+-ion vacancies. In consequence, the dominant components of the absorption and the C_1/C_2 luminescence bands of Ce^{3+} in KMF are strongly associated with T_1 and R_1 estimated from the ESR results.

K^+-ion vacancies close to Ce^{3+} produce odd-parity distortions of the Ce^{3+} complexes, which lower symmetry and enhance the crystal field splitting of the $5d^1$ excited state, resulting in a red shift of the absorption and luminescence. This effect can explain the experimental result that the peaks of the B_1/B_2 luminescence bands are shifted to lower energy than those of the C_1/C_2 luminescence bands. In consequence, the weak B_1/B_2 luminescence bands correspond to the T_2 centre with a K^+-ion vacancy near to Ce^{3+}.

Finally, we consider a model of R_2. The ESR results show that a Ce^{3+} ion substitutes for a Mg^{2+} ion with a vacancy at the nearest neighbour Mg^{2+} site along the [101] direction. Luminescence from R_2 is expected to be observed at different energy region because of a six-fold coordination. The luminescence band in Ce^{3+}:$KCaF_3$ where Ce^{3+} may substitute for Ca^{2+} in a six-fold coordination was observed at 408 nm [22]. However, such luminescence could not be observed in Ce^{3+}:KMF at room temperature. It may be due to a large non-radiative decay rate at room temperature. In order to confirm such luminescence in Ce^{3+}:KMF, low-temperature experiments are required.

4.4. Comparison of KMF with BLF

4.4.1. ESR The T_1 centre in KMF is assigned to Ce^{3+} with the vacancy away from Ce^{3+}, whereas that in BLF is assigned to Ce^{3+} accompanied by the Li^+ substitution at the nearest neighbour Ba^{2+} sites along the [001] directions. Both T_1 centres show nearly cubic symmetry and their ground-state eigenfunctions are approximate to Γ_7, of which the dominant component is $|\frac{5}{2}, \pm\frac{5}{2}\rangle$.

Both T_2 centres in KMF and BLF are assigned to Ce^{3+} with the vacancies at the nearest neighbour K^+ and Ba^{2+} ions along the [001] direction, respectively. However, their eigenfunctions are different. The dominant components of the eigenfunctions are $|\frac{5}{2}, \pm\frac{5}{2}\rangle$ for KMF, and $|\frac{5}{2}, \pm\frac{1}{2}\rangle$ for BLF. The ground-state eigenfunctions of $|\frac{5}{2}, \pm\frac{5}{2}\rangle$ and $|\frac{5}{2}, \pm\frac{1}{2}\rangle$ mean that the sign of the coefficient B_2^0 of the axial crystal field interaction $B_2^0 O_2^0$ is negative and positive, respectively [8,14]. The sign of B_2^0 can deduce that Ce^{3+} complexes are compressed and elongated along the axial distortion. The valence of +3 for a pair of Ce^{3+}-vacancy in KMF and BLF has an excess and less of 1 for pairs of K^+-K^+ and Ba^{2+}-Ba^{2+}, respectively. Such valence difference seems to cause compression and elongation of the Ce^{3+} complexes in KMF and BLF, respectively.

The R_1 and R_2 centres in BLF are assigned to Ce^{3+} accompanied by the Li^+ substitution and a Ba^{2+}-ion vacancy at the nearest neighbour Ba^{2+} site along the [110] direction, respectively [8]. As the models for the R_1 and R_2 centres in KMF are different from those in BLF, we do not discuss the ESR results between these centres.

4.4.2. Optical The B and C luminescence bands were observed in KMF, whereas the A, B and C luminescence bands were observed in BLF. The C luminescence bands for KMF and BLF have the medium Stokes shift energies of $\sim$4500 and $\sim$4400 cm^{-1}, respectively, and the same lifetimes of 20 ns [7]. This indicates that Ce^{3+} ions in KMF and BLF substitute for K^+ and Ba^{2+} ions with nearly cubic twelve-fold coordinations. The C luminescent centres are assigned to T_1 and R_1 in KMF and to R_1 in BLF. As the distance ($\sqrt{2}a$) between Ce^{3+} and Li^+ for R_1 in BLF is large, such Li^+ substitution is less effective for the distortions of the Ce^{3+} complexes, giving rise to nearly cubic symmetry. Both B luminescence bands in KMF and BLF have a red shift. They are assigned to the T_2 centres.

The intense A luminescence band observed only in BLF has the large Stokes shift energy ($\sim$8300 cm^{-1}) [7,9]. The A luminescent centre in BLF is assigned to the T_1 centre. The Li^+ substitution along the [001] direction for the T_1 centre in BLF is expected to produce a large lattice relaxation of the $5d^1$ excited state of Ce^{3+}, resulting in the large Stokes shift [9].

In consequence, the big difference in KMF and BLF is to add the Li^+ substitution in BLF other than the cation vacancies as the charge compensators.

5. Conclusions

The ESR results of Ce^{3+} in KMF identify four Ce^{3+} centres accompanied by different charge compensators; Ce^{3+} ions substituting for K^+ ions away from and near to K^+-ion vacancies, and for a Mg^{2+} ion with a vacancy of the nearest neighbour Mg^{2+} ion along the [101] direction. The C and B luminescence bands of Ce^{3+} in KMF with the different peak energy and Stokes shift energy were observed. The Ce^{3+} centres away from the K^+-ion vacancies correspond to the C luminescence bands with the medium Stokes shift energy ($\sim$4500 cm^{-1}). On the other hand, the Ce^{3+} centre strongly distorted by the K^+-ion vacancy near to Ce^{3+} is associated with the B luminescence bands with a red shift and the large Stokes shift energy ($\sim$6800 cm^{-1}).

Acknowledgments

This work was partially supported by the Research for the Future Program 'Growth and characterization of single crystals for active elements' of Japan Society for the Promotion of Science.

References

[1] Ehrlich T D J, Moulton P F and Osgood R M 1978 *Opt. Lett.* **4** 184
[2] Okada F, Togawa S and Ohta K 1994 *J. Appl. Phys.* **75** 49
[3] Marshall C D, Speth J A, Payne S A, Krupke W F, Quarles G J, Castillo V and Chai B H T 1994 *J. Opt. Soc. Am.* B **11** 2054
[4] Kodama N, Yamaga M and Henderson B 1998 *J. Appl. Phys.* **84** 5820
[5] Dubinskii M A and Schepler K L 1998 *J. Mod. Opt.* **45** 221
[6] Combes C M, Dorenbos P, van Eijk C W E, Gesland J Y and Ridnyi P A 1995 *J. Lumin.* **72–74** 753
[7] Yamaga M, Imai T, Shimamura K, Fukuda T and Honda M 2000 *J. Phys.: Condens. Matter* **12** 3431
[8] Yamaga M, Honda M, Shimamura K, Fukuda T and Yosida T 2000 *J. Phys.: Condens. Matter* **12** 5917
[9] Marsman M, Andriessen J and van Eijk C W E 2000 *Phys. Rev.* B **61** 16477
[10] Francini R, Grassano U M, Landi L, Scacco A, D'Elena M, Nikl M, Cechova N and Zema N 1997 *Phys. Rev.* B **56** 15 109
[11] Ibragimov I R, Fazlizhanov I I, Falin M L and Ulanov V A 1992 *Fiz. Tverd. Tela.* (St. Petersburg) **34** 3261
Ibragimov I R, Fazlizhanov I I, Falin M L and Ulanov V A 1992 *Sov. Phys. Solid State* **34** 1745
[12] Wojtowicz A J, Szupryczynski P, Glodo J, Drozdowski W and Wisniewski D 2000 *J. Phys.: Condens. Matter* **12** 4097
[13] Yamaga M, Imai T and Kodama N 2000 *J. Lumin.* **87–89** 992
[14] Abragam A and Bleaney B 1970 *Electron Paramagnetic Resonance of Transition Ion* (Oxford: Clarendon)
[15] Yamaga M, Imai T, Miyairi H and Kodama M 2000 *J. Phys.: Condens. Matter* **13** 753
[16] Kaminskii A A 1990 *Laser Crystals* (Berlin: Springer) table 2.1
[17] Rubins R S 1970 *Phys. Rev* B **1** 139
[18] Henderson B and Imbusch F G 1989 *Optical Spectroscopy of Inorganic Solids* (Oxford: Clarendon) ch. 2
[19] McLaughlan S D and Forrester P A 1966 *Phys. Rev.* **151** 311
[20] Weger M 1960 *Bell Syst. Tech. J.* **39** 1013
[21] Verweji J W M, Pedrini C, Bouttet D, Dujardin C Lautesse H and Moine B 1995 *Opt. Mater.* **4** 575
[22] Mazurak Z, Ratuszna A, Paniel Ph 1999 *J. Lumin.* **82** 163